Atmos. Chem. Phys. Discuss., 13, 2997–3029, 2013
www.atmos-chem-phys-discuss.net/13/2997/2013/
doi:10.5194/acpd-13-2997-2013

Atmospheric Chemistry and Physics
Discussions
Open Access

Aerosol effects on the cloud-field properties of tropical convective clouds

S.-S. Lee[1] and G. Feingold[2]

[1]NOAA Earth System Research Laboratory, Chemical Sciences Division, Boulder, Colorado, USA
[2]Cooperative Institute for Research in Environmental Sciences (CIRES), University of Colorado, Boulder, Colorado, USA

Received: 17 January 2013 – Accepted: 21 January 2013 – Published: 30 January 2013

Correspondence to: S.-S. Lee (seoung.soo.lee@noaa.gov)

Published by Copernicus Publications on behalf of the European Geosciences Union.

Abstract

Aerosol effects on condensed water and precipitation in a tropical cloud system driven by deep convective clouds are investigated for two-dimensional simulations of two-day duration. Although an assumed ten-fold increase in aerosol concentration results in a similar temporal evolution of mean precipitation and a small (9 %) difference in cumulative precipitation between the high- and low-aerosol cases, the characteristics of the convection are much more sensitive to aerosol. The convective mass flux, and temporal evolution and frequency distribution of the condensed water path WP (sum of liquid and ice water paths) differ significantly between unperturbed and aerosol-perturbed simulations. There are concomitant differences in the relative importance of individual microphysical processes and the frequency distribution of the precipitation rate (P). With increasing aerosol, (i) the convective mass flux increases, leading to increases in condensation, cloud liquid, and accretion of cloud liquid by precipitation; (ii) autoconversion of cloud water to rain water decreases; (iii) the WP spatial distribution becomes more homogeneous; (iv) there is an increase in the frequencies of high and low WP and P and a decrease in these frequencies at the mid-range of WP and P. Thus while aerosol perturbations have a negligible influence on total precipitation amount, for the case considered, they do have substantial influence on the spatiotemporal distribution of convection and precipitation.

1 Introduction

Aerosol-cloud interactions are known to have strong bearing on climate change, however, the impact of these interactions on climate has not been quantified adequately (Solomon et al., 2007). Among numerous pressing issues is the need to evaluate aerosol effects on mixed-phase convective clouds. These clouds are one of the important components of the global hydrological circulation and the climate system.

Early investigations of aerosol interactions with deep convective clouds tended to focus on a single cloud cell of short duration (hours) (Flossmann, 1991; Respondek et al., 1995; Orville et al., 2001). However, it is known that global hydrological circulations and climate are strongly controlled by cloud systems which comprise multiple clouds and last many days (Houze, 1993). The availability of powerful computing has afforded the possibility to explore long-term (multiple days to months), large-domain simulations of convective cloud systems, along with the promise of a much more realistic view of potential aerosol influences on these systems. Cloud system studies of long duration or encompassing large domains have demonstrated that total precipitation amount is predominantly determined by radiative-convective equilibrium (RCE) or the applied large-scale forcing, which leads to negligible variations of the precipitation amount with varying aerosol (Grabowski, 2006; van den Heever et al., 2011; Morrison and Grabowski, 2011).

The question posed here is whether the aerosol has any impact on the spatiotemporal characteristics and frequency distribution of the precipitation? The answer requires exploration of known aerosol influences on the microphysical properties of clouds and the pathways via which precipitation forms. For example, for a small change in precipitation, the aerosol-induced suppression of the conversion of cloud liquid to rain via collisions among droplets (i.e. autoconversion) must be compensated by increases in other cloud-liquid and cloud-ice precipitation-production pathways, each having different characteristic timescales. Thus, aerosol-induced compensation mechanisms are likely to involve changes in the magnitude and, possibly, spatiotemporal distribution of air mass flux (a function of dynamics) and associated mass of cloud liquid and cloud ice. These ideas find support in recent studies (e.g. van den Heever et al., 2011; Wang et al., 2011; Fan et al., 2012) which have shown that despite negligible influence on total precipitation amount, the variations of precipitation and WP spatiotemporal distribution and frequency induced by aerosol acting as cloud condensation nuclei were substantial. Earlier studies have also shown that aerosol acting as a heat source can alter the spatiotemporal distribution of air mass fluxes and thus that of cloud liquid,

ACPD
13, 2997–3029, 2013

cloud ice and precipitation (Kim et al., 2006; Meehl et al., 2008). It is important to note that over the global scale and sufficiently long period of time, precipitation and evaporation must balance at the surface. Hence, aerosol influences on precipitation and associated WP distribution are more relevant to the assessment of local or regional precipitation patterns than to total precipitation amount. For example, as shown in the Sahel drought, aerosol-induced changes in precipitation distribution have strong societal and economic impacts (Batterbury and Warren, 2001; Lee, 2011).

Motivated by the importance of the effect of aerosol on precipitation and WP distribution, this paper documents aerosol effects on the spatiotemporal distribution of clouds and precipitation in a mesoscale system comprising multiple deep convective clouds. Henceforth, this type of mesoscale system is referred to as a mesoscale cloud ensemble (MCE; Houze, 1993).

A comprehensive approach to aerosol-cloud-precipitation interactions requires simulations that are of long enough duration (as high as RCE timescales) and on a global scale, to allow the cloud system to evolve at the full range of scales (Grabowski, 2006; Tao et al., 2012). Idealized simulations on more limited spatiotemporal scales are nevertheless of great value since they allow more detailed resolution of convective and microphysical processes on timescales relevant to the duration of aerosol perturbations. Using an idealized framework, this study attempts to further our understanding of changes in the spatiotemporal distribution of clouds and precipitation induced by aerosol.

2 Cloud-system resolving model (CSRM)

The Goddard Cumulus Ensemble (GCE) model (Tao et al., 2003), a two-dimensional nonhydrostatic compressible model, is used here as a cloud-system resolving model. Shortwave and longwave radiation parameterizations have been included in all simulations. The microphysical processes are represented by a double-moment bin-bulk scheme that uses bin-model-derived lookup tables for hydrometeor collection

ACPD
13, 2997–3029, 2013

processes (Saleeby and Cotton, 2004). A gamma size distribution with fixed breadth is assumed for hydrometeor size distributions. Cloud-droplet and ice-crystal nucleation also mimic a size-resolved approach (Lee et al., 2010). Aerosol is represented by a single scalar (number mixing ratio) and the assumption of a fixed (lognormal) size distribution. During the simulation, aerosol is advected, diffused and depleted. Through droplet or ice nucleation, aerosol mass is included in cloud liquid or cloud ice and is transferred to other species of hydrometeors through collection. Aerosol mass moves from the atmosphere to the surface when precipitating hydrometeors fall to the surface and aerosol mass is released from hydrometeors to the atmosphere when hydrometeors evaporate or sublimate (Feingold and Kreidenweis, 2002).

The effects of aerosol, both unactivated and activated, on radiative heating (i.e. aerosol direct and semi-direct effects) are not taken into account.

3 Case description

Two-day two-dimensional simulations of an observed mesoscale cloud ensemble (MCE; Houze, 1993) are performed over a two-day period. The MCE was observed during a part of the Tropical Warm Pool-International Cloud Experiment (TWP-ICE) (12:00 LST (local solar time) 23 January–12:00 LST 25 January 2006) campaign in Darwin, Australia (12.47° N, 130.85° W), as described by May et al. (2008) and Fridlind et al. (2009).

Large-scale forcing for potential temperature and specific humidity is applied to the model every time step by interpolating the 3-hourly observed soundings. The observed, temporally-varying surface fluxes of heat and moisture are prescribed uniformly across the surface, and are identical for all simulations. This method of modeling cloud systems was used for the CSRM comparison study by Xu et al. (2002). The details of the procedure for applying large-scale forcings are described in Donner et al. (1999). The horizontal momentum is damped to observed values, following Xu et al. (2002).

ACPD
13, 2997–3029, 2013

The simulations of the observed MCE have the same fundamental configuration. The horizontal domain length is set at 256 km in the east-west direction to capture mesoscale structures of the storm while the vertical domain length is set at 20 km. The horizontal (vertical) grid length is 500 (200) m. Periodic boundary conditions are applied on horizontal boundaries.

Initial background aerosol profiles, observed during the concurrent Aerosol and Chemical Transport in tropIcal conVEction (ACTIVE) program (Vaughan et al., 2008) are adopted by the control run. The initial size distribution and number concentration of background aerosol are identical to those in Fig. 4 in Fridlind et al. (2009). The average background aerosol number concentration (integrated over the distribution) and over the PBL is $\sim 400\,\mathrm{cm}^{-3}$. Background aerosol concentration is $\sim 450\,\mathrm{cm}^{-3}$ at the surface and decreases monotonically to $\sim 350\,\mathrm{cm}^{-3}$ at the top of the PBL. To examine the aerosol effect, the control run is repeated but only the aerosol number concentration is enhanced by a factor of 10. This simulation is referred to as the "high-aerosol run". This rather significant perturbation reflects something akin to a major biomass-burning event rather than a sustained perturbation over the course of months; it is therefore appropriate for the relatively short two-day simulations. To test the robustness of results to lower aerosol perturbations, the control run is repeated with aerosol number concentration enhanced by a factor of 3; this simulation is referred to as "the medium-aerosol run".

4 Results

4.1 Precipitation, condensation and updrafts

Figure 1 depicts the time series of the area-mean rainrate P smoothed over 3 h for all simulations, compared to observations. As expected, the precipitation is simulated reasonably well because of the strong meteorological control on P. The averaged cumulative precipitation over the domain at the last time step for the high-aerosol run and the

ACPD
13, 2997–3029, 2013

medium-aerosol run is 95.7 mm and 90.1 mm, which is $\sim 9\,\%$ and $\sim 2\,\%$ greater than that for the control run, respectively. Increasing the aerosol concentration enhances precipitation but these differences in precipitation are quite small as compared to the ten- and three-fold increases in aerosol concentration. This is similar to findings in Grabowski (2006), van den Heever et al. (2011) and Morrison and Grabowski (2011).

Following Lee et al. (2008a), we calculate differences in the domain-average cumulative sources and sinks of the sum of precipitable hydrometeors between the high-aerosol run and control run (high aerosol-control) and between the medium-aerosol run and control run (medium aerosol-control) to elucidate the microphysical processes leading to the small difference in total precipitation amount. Among the sources and sinks, autoconversion and terms associated with accretion of cloud liquid account for the primary differences in the precipitation amount (Lee et al., 2008b; Lee and Feingold, 2010). The aerosol-induced increase in accretion of cloud liquid by precipitation and cloud ice offsets the aerosol-induced decrease in autoconversion to yield a small difference in the precipitation amount.

The presence of increased cloud liquid is required for the increase in accretion. As shown in Lee et al. (2008b), there are substantial (30–40 %) increases in condensation and associated cloud liquid. These increases are slightly greater than increases in evaporation and associated cloud-liquid loss. This leads to increases in accretion that are slightly larger than decreases in autoconversion, leading to the slight increases in the precipitation amount with increasing aerosol concentration. It is noteworthy that none of the primary budget terms includes the less well-known cloud-ice and ice-ice interactions, however this may change in the future as our knowledge of these processes improves.

The precipitation efficiency (cumulative precipitation normalized with respect to cumulative condensation at the end of time integration) is 0.40, 0.45 and 0.51 in the high-, medium- and control runs, respectively. The high- and medium-aerosol runs produce slightly larger cumulative precipitation in spite of the lower efficiency of rain production (Lee and Feingold, 2010). The small increase in the precipitation amount in this system

ACPD
13, 2997–3029, 2013

S.-S. Lee and G. Feingold

is made possible by the substantial increase in condensation, which dominates the reduced efficiency with which cloud liquid is converted to precipitation. Condensation is closely linked to the dynamic intensity of a system, which suggests that we should see commensurate response in metrics of the system dynamics. Figure 2a and b shows the time- and domain-averaged vertical distribution of updraft mass fluxes and the time series of the average updraft mass fluxes. The high- and medium-aerosol runs show significantly increased updraft mass fluxes, consistent with substantially increased condensation.

Figure 1b shows the frequency distribution of P. Although variations in cumulative precipitation between the three runs are very small for the strong aerosol perturbations, the frequency distribution of P shows features that clearly differentiate the high-, or medium-aerosol run from the control run (Fig. 1b). For the interpretation of this analysis, P is classified as light ($P < 5\,\mathrm{mm\,h^{-1}}$), moderate ($P$ between 5 and $15\,\mathrm{mm\,h^{-1}}$), and heavy ($P > 15\,\mathrm{mm\,h^{-1}}$). The most conspicuous differences in the precipitation frequency distribution between the runs are (i) for the heavy P between $\sim 15\,\mathrm{mm\,h^{-1}}$ and $\sim 28\,\mathrm{mm\,h^{-1}}$, the high- and medium-aerosol run have $\sim 40\,\%$ and $\sim 25\,\%$ larger precipitation frequency than the control run, respectively. Precipitation rates $> 28\,\mathrm{mm\,h^{-1}}$, although relatively rare in the perturbed simulations, do not exist in the control simulation; (ii) for light precipitation, the high- and medium-aerosol run show on average $\sim 30\,\%$ and 20 % larger frequency than the control run, respectively; and (iii) for moderate rainrates, the control run shows on average $\sim 35\,\%$ and 21 % larger precipitation frequency than the high- and medium-aerosol runs, respectively. The high- and medium-aerosol runs respond to the aerosol perturbation in a qualitatively similar way (Figs. 1 and 2, discussions in this section, as well as further analyses pertaining to subsequent sections). Hence, results from the high-aerosol and control runs will hereafter be the focus of analysis and discussion.

ACPD
13, 2997–3029, 2013

4.2 Water path

4.2.1 Time series, frequency distribution, and power spectral analysis

We showed in the previous section that condensation and evaporation are altered by aerosol significantly. Since condensation and evaporation are dominant source and sink of cloud mass, we explore aerosol influences on condensed cloud mass, as represented by liquid-water path (LWP) and ice-water path (IWP). Figure 3a shows the time series of the domain-averaged LWP and IWP over the simulation period. It is clear that LWP accounts for most of the water path (WP = LWP + IWP) and that the LWP differences are correlated with the precipitation differences, albeit with a lag of ~ 40 min (cf. Figs. 1a and 3a). This lag time is associated with the delay time required for precipitation to form and fall to the ground.

Figure 3b shows the frequency distribution of WP. As in the case of P, the high-aerosol run is characterized by (i) a higher frequency of high WP (> 1000 $\mathrm{g\,m^{-2}}$); (ii) a lower frequency of events in the mid range of WP between ~ 100 and 1000 $\mathrm{g\,m^{-2}}$; and (iii) a higher frequency of low WP (< 100 $\mathrm{g\,m^{-2}}$) (cf. Fig. 1b). It is worth pointing out that there is also a higher frequency of high cloud-top heights (> 8 km), a lower frequency of mid cloud-top heights between 4 km and 8 km, and a higher frequency of low cloud-top heights (< 4 km) in the high-aerosol run. This indicates a correlation between the WP and cloud-top height distributions.

Grid columns with a specific P are collected over the course of the two-day simulation Then, the mean and the standard deviation of WP over these columns are calculated. This calculation is performed for P between 0 and 45 $\mathrm{mm\,h^{-1}}$, discretized into linearly distributed bin values. Note that 45 $\mathrm{mm\,h^{-1}}$ corresponds to the maximum precipitation rate in the two simulations. Figure 4 shows the mean and standard deviation of WP for the discretized P between 0 and 45 $\mathrm{mm\,h^{-1}}$. Figure 4 demonstrates that, as expected, larger P is associated with larger WP, consistent with the correlations in differences in WP and those in P in Figs. 1 and 3. It is noteworthy that the rate of the P increase with increasing WP is higher in the control run. Stated differently, the clean aerosol

ACPD
13, 2997–3029, 2013

conditions produce higher Ps than the high-aerosol conditions for the same WP. This reflects the higher precipitation efficiency in clean conditions as discussed in depth in Lee and Feingold (2010).

Figure 5a shows the power spectral analysis based on the domain-averaged WP time series (Fig. 3a). First, at the lowest frequencies (spatial scales ~ 250 km based on the average advection speed of 10 m s^{-1}), the high-aerosol run exhibits larger spectral power; second, it is notable that in the high-aerosol run, the power is larger, and distributed more homogeneously for frequencies $>\sim 1.6 \times 10^{-4}$ Hz (spatial scales $<\sim 70$ km). However, between $\sim 0.5 \times 10^{-4}$ and $\sim 1.6 \times 10^{-4}$ Hz, the control run exhibits greater power. Similar to these differences in the WP power, when the power spectral analysis is performed on the updraft-mass-flux time series (Fig. 2b), the high-aerosol run has larger power throughout the frequency range except for that between $\sim 0.8 \times 10^{-4}$ and $\sim 1.8 \times 10^{-4}$ Hz (Fig. 5b).

4.2.2 Homogeneity

Following Barker (1996), a nondimensional homogeneity parameter H_σ is used to quantify the spatial homogeneity of cloud fields. H_σ is defined as $(\overline{A}/\sigma_A)^2$ where $\overline{A}$ and σ_A represent the spatial mean and standard deviation of A at a certain time, respectively, and A denotes the variable under consideration. H_σ of WP is calculated at each time step and the time series of H_σ is shown in Fig. 6. Throughout the simulation period, H_σ of the high-aerosol run exceeds that of the control run.

It is interesting to examine the differences in the spatial distribution of WP when differences in the homogeneity between the two runs are either at their maximum or their minimum during the simulation period (Fig. 7a, b). The maximum and minimum differences in homogeneity between the two simulations occur around 02:00 LST and 12:00 LST on 24 January (marked by arrows in Fig. 6), respectively. At the time of the maximum difference in H_σ, WP fluctuates with little deviation around ~ 3500 g m^{-2} in the high aerosol run. However in the control run, WP varies widely from 0 to ~ 10 000 g m^{-2} associated three distinct peaks in WP (Fig. 7a). At the time of the minimum difference in the WP homogeneity (Fig. 7b), WP is generally larger in the high-aerosol run. However, in contrast to Fig. 7a, there are no distinct differences in the WP spatial variations between the simulations.

The much larger homogeneity of WP in the high-aerosol run at the time of the maximum H_σ difference is reflected in the power spectral analysis on the spatial distribution of WP over the domain. (Note that this differs from the power spectra calculated from the domain-averaged time series in Fig. 5.) Fig. 8a shows that at the time of the maximum difference in H_σ the spectral power in the high-aerosol run concentrates at small wavenumbers (k); it exhibits much less variability compared to the control run than in the range between ~ 0.05 and $0.25\,\mathrm{km}^{-1}$ (or ~ 4 to $20\,\mathrm{km}$ when translated to a spatial scale). In this range, the control run power spectrum exhibits a distinct peak around $k = 0.12\,\mathrm{km}^{-1}$ ($\sim 8\,\mathrm{km}$) and a large decrease in the power thereafter. Overall the perturbed case concentrates more energy in the smallest and largest wavenumbers. These differences are consistent with the homogeneous spatial variation of WP for the perturbed case at the time of the maximum difference (Fig. 7a).

At the time of minimum difference in homogeneity, the difference in the distribution of power over the entire k range between the high-aerosol and control runs is relatively small, although there is a slight decrease in power for k of $\sim 0.1\,\mathrm{km}^{-1}$ or above in the control run.

The WP frequency distribution at the time of maximum differences in homogeneity (Fig. 9a) is much wider in the control run, as expected from Fig. 7a. While in the high aerosol run, convective cells with moderate WP are spread throughout the domain, in the control-run, convective cells with very large WP are interspersed with those with very small WP (Figs. 7a and 9a). This reflects substantial aerosol-induced changes in cloud-field properties. At the time of minimum homogeneity difference (Fig. 9b), the WP frequency is spread over a similar range for both of the runs, with a shift to larger WP values in the perturbed case, as expected from Fig. 7b.

ACPD
13, 2997–3029, 2013

4.2.3 Temporal evolution of the WP frequency

The WP frequency distribution is now calculated for three separate time segments over the course of the two-day simulation. The first, second and third segments are 12:00 LST on 23 January–00:00 LST on 24 January, 00:00 LST on 24 January–18:00 LST on 24 January and 18:00 LST on 24 January–12:00 LST on 25 January, respectively. The segments correspond to initial, mature and decaying stages of convective activity based on the precipitation evolution in Fig. 1a. Precipitation starts and increases in the initial stage and reaches its maximum value in the mature stage. In the decaying stage, precipitation stabilizes to a low level and does not vary much.

For the first segment, there are significant differences in the WP frequency for WP between 0 and $\sim 100\,\mathrm{g\,m^{-2}}$ (Fig. 1a), however, there are negligible differences for WP $>\sim 100\,\mathrm{g\,m^{-2}}$. In the second segment, significant differences in the WP frequency distribution are evident (Fig. 1b) with a tendency for the perturbed simulation to be characterized by more frequent higher, and fewer small WP events. In the third segment, the distributions qualitatively resemble those in the second segment (Fig. 1c) although both are narrower, particularly that of the perturbed simulation. Note that there are no occurrences of WP $< 100\,\mathrm{g\,m^{-2}}$ for both of the runs. Figure 1 shows that the difference in the occurrence of low WP $<\sim 100\,\mathrm{g\,m^{-2}}$ appears during the initial stage, while the difference in the occurrence of moderate WP clouds with $100\,\mathrm{g\,m^{-2}} <$ WP $< 1000\,\mathrm{g\,m^{-2}}$ occurs during the mature stage. For clouds with high WP $> 1000\,\mathrm{g\,m^{-2}}$, the difference is mostly manifested during the mature and decaying stage of convective activity.

4.2.4 Radiation

The time- and domain-averaged shortwave and longwave fluxes at the top of domain are 109.2 and $129.5\,\mathrm{W\,m^{-2}}$, respectively, in the high-aerosol run Here, minus and plus represent downward and upward fluxes, respectively. The equivalent shortwave and longwave fluxes in the control run are -118.5 and $133.2\,\mathrm{W\,m^{-2}}$ With increasing aerosol, net radiation fluxes at the domain top (i.e. shortwave plus longwave fluxes) increase

Discussion Paper | Discussion Paper | Discussion Paper | Discussion Paper |
ACPD
13, 2997–3029, 2013

from 14.7 to 20.3 $W\,m^{-2}$, mainly due to more reflection of incident shortwave radiation at the top in the high-aerosol run. However, it should be pointed out that ~ 40 % of the increase in the reflection of shortwave radiation is offset by a decrease in the outgoing longwave radiation at the top with increasing aerosol. This offset is an order of magnitude larger than that in warm stratocumulus clouds (e.g. Lee et al., 2009).

Figure 11a shows vertical distributions of the time- and domainaveraged radiative heating rates. Net heating rates (i.e. shortwave plus longwave heating rates) show generally larger and smaller heating above and below ~ 5 km, respectively, in the high-aerosol run (Fig. 11a). The larger heating above 5 km dominates the smaller heating below 5 km in the high-aerosol run, leading to the larger time- and domain-averaged net heating (−1.23 $K\,h^{-1}$) than in the control run (−1.41 $K\,h^{-1}$). Comparisons amongst Fig. 11a–c demonstrate that differences in the net heating between the runs are mostly caused by those in longwave heating. They also show that the time- and domain-averaged shortwave heating is lower in the high-aerosol run and thus the larger net heating is enabled by higher longwave heating in the high-aerosol run.

Figure 12a shows the vertical distribution of the time- and domain-averaged sum of liquid-water and ice-water content. Above ~ 9 km, the level of homogeneous freezing, most of the sum is accounted for by ice water, while below ~ 9 km most is accounted by liquid water. Figure 12b shows the vertical distribution of the time-and domain-averaged net longwave flux. Larger net longwave flux in the high-aerosol run becomes smaller than that in the control run around 10 km due to larger ice mass blocking more upward longwave flux. This induces the smaller outgoing longwave radiation at the model top and plays a critical role in the larger longwave heating.

Figure 3c shows the frequency distribution of WP from the repeated control and high-aerosol runs with explicit radiation calculations turned off but with the averaged heating rate from the high-aerosol run (shown in Fig. 11a) imposed on all grid points in both of the repeated runs. Hence, there are no differences in radiative heating between the repeated runs. There are no qualitative differences between Fig. 3b, c, which exemplifies

ACPD
13, 2997–3029, 2013

that aerosol-induced changes in radiative heating rates do not influence the qualitative nature of results discussed in the previous sections.

5 Discussion

5.1 Updraft mass flux

This study shows that mass fluxes associated with the high aerosol run are approximately 2 times larger than those from the low aerosol run (Fig. 2). In contrast, Morrison and Grabowski (2011) show negligible differences in updraft mass fluxes between their high- and low-aerosol experiments for the same TWP-ICE case. Their high aerosol case has ~ 20 times larger aerosol concentration than their low aerosol case. This implies that in their simulations the increase in condensation (in response to that in updrafts) and the subsequent increase in accretion of cloud liquid may not be a primary compensation mechanism. (Note that Morrison and Grabowski, 2011 also showed a nearly identical precipitation amount between the high- and low-aerosol cases.) However, in agreement with this study, van den Heever (2011) simulated ~ 2 times larger updrafts with 16 times higher aerosol concentration for tropical clouds in radiative convective equilibrium (RCE). Morrison and Grabowski (2011) and this study adopt different simulation setups (e.g. resolution and domain size) and different microphysics parameterizations. Van den Heever (2011) and this study use approximately the same microphysical scheme. To gain a more comprehensive understanding of the mass flux response and the compensation mechanism, future work will examine the sensitivity of the mass-flux response to the simulation setup and microphysics parameterization.

5.2 Precipitation frequency

Previous studies (e.g. Fan et al., 2012; van den Heever et al., 2011; Wang et al., 2011; Koren et al., 2012; Li et al., 2011) examining the response of the *P* frequency to aerosol in deep convective clouds reaching the tropopause used different criteria to classify *P*.

ACPD
13, 2997–3029, 2013

Note that while Fan et al. (2012), van den Heever et al. (2011) and Wang et al. (2011) rely on models for the P-frequency calculation, Koren et al. (2012) and Li et al. (2011) used ground-based and satellite observations for their calculations. The maximum P in those studies are different to this study, as are the classifications into P ranges. The significantly different classifications exacerbate comparisons among studies. Nevertheless, the abovementioned previous studies and this study all show a tendency for aerosol perturbations to shift the PDF of P to the largest P class. In other words, there is good agreement amongst studies that an increase in aerosol enhances the frequency of relatively heavy precipitation. However, in other ranges of P, there are discrepancies in the response of the P frequency. This may not be that surprising considering significant differences in the development stages of convection and environmental conditions among studies and the strong dependence of cloud and precipitation characteristics on these conditions and stages (Weisman and Klemp, 1982; Houze, 1993).

5.3 RCE

It is well known that it takes ~ 20 days for a tropical convective system to reach RCE (Tompkins and Craig, 1998), whereas this study considers a two-day simulation period. Hence, we do not address aerosol-cloud interactions in RCE where the implications of aerosol-cloud interactions for climate might emerge. However, interestingly, there are similarities between this study and previous studies in RCE (e.g. van den Heever et al., 2011; Grabowski, 2006): (i) van den Heever et al. (2011), Grabowski (2006) and this study, not surprisingly, show very weak changes to domain-averaged cumulative precipitation (ii) these studies all show significant changes in updraft mass fluxes and the P frequency distribution due to aerosol perturbation, although there are quantitative differences in changes in P frequency distribution. A likely cause of these quantitative differences is the disparity in time available for radiation-cloud interactions to manifest (Zeng et al., 2007; Lee et al., 2012).

ACPD
13, 2997–3029, 2013

S.-S. Lee and G. Feingold

5.4 Raindrop terminal velocity

Recent studies have linked the characteristics of a convective system to the raindrop terminal velocity (Parodi et al., 2011; Parodi and Emanuel, 2009). Their simulations that differ only in the specification of the raindrop terminal velocity show that cloud size decreases while updraft strength increases with increasing raindrop terminal velocity. The current model simulations apply the appropriate fall velocities to all precipitating particles based on their temporally and spatially varying mean size. However, to compare our results to these earlier studies we have calculated the average raindrop terminal velocity for control and perturbed simulations: these are respectively $6.5\,\mathrm{m\,s^{-1}}$ and $7.8\,\mathrm{m\,s^{-1}}$ (temporally and domain-averaged over all regions with mass mixing ratio $> 0.05\,\mathrm{g\,kg^{-1}}$). Since raindrop terminal velocity is smaller in the control run than in the high-aerosol run, our results are qualitatively consistent with Parodi et al. (2011) and Parodi and Emanuel (2009): as a result of the aerosol perturbation, the average cloud radius (based on liquid-phase cloud entities) decreases from 7.1 km to 5.6 km. This broad consistency reinforces the conclusion by Parodi et al. (2011) and Parodi and Emanuel (2009) that raindrop terminal velocity is a fundamental physical parameter that is able to explain variability in the properties of a convective system.

6 Summary and Conclusions

The effects of aerosol on a tropical cloud system driven by deep convection have been investigated. The difference in total precipitation resulting from a 10-fold increase in aerosol concentration is only 9 % due to compensation among microphysical pathways. While the aerosol perturbation suppresses autoconversion, there is a substantial increase in accretion of cloud liquid by precipitation, which results in the small variation of total surface precipitation. This increase in accretion is due to a significant increase in updraft mass fluxes and condensation.

ACPD
13, 2997–3029, 2013

S.-S. Lee and G. Feingold

Although total precipitation amounts are similar, there is a significant difference in the frequency distribution of P; with increasing aerosol, there is a marked increase in the occurrence of light and heavy rain, while there is a notable decrease in moderate rain. Changes in the frequency distribution of WP and cloud-top height are qualitatively similar. A strong similarity in the response of the spectral power of the timeseries of WP and that of updrafts to aerosol perturbation is noted. This similarity indicates that a change in the power of the temporal scale of cloud mass due to an aerosol perturbation tends to be associated with the temporal scale of updrafts.

Most of the differences in the WP frequency at the lower bound of the WP range are noticeable during the early stage of convective activity, while the differences in the WP frequency in the middle WP range emerge during the mature stage of convective activity The differences in the WP frequency at the upper WP range are manifested during the middle and decaying stages of convective activity.

Increases in the aerosol also result in a significant increase in the spatial homogeneity of the water condensate for most of the simulation period. The differences in the spatial variation, frequency and power of the WP are substantial at the time of the maximum difference in homogeneity, but significantly less so at the time of the minimum difference.

The difference between the temporal evolution of the WP in high-aerosol and control runs is strongly correlated with that of the precipitation difference, albeit with a lag of ~ 40 min.

With increasing aerosol, less radiation enters the domain due to more reflection of incident solar radiation. However, a significant portion of the increase in the reflected radiation is offset by more longwave radiation trapped by increasing ice mass in the upper troposphere. It is notable that longwave radiative heating gets higher, which makes net radiative heating higher with increasing aerosol. Hence, aerosol-induced changes in longwave radiation tend to compensate for aerosol-induced decreases in solar radiation and associated cooling. However, these changes in radiative heating do not have significant impacts on the qualitative nature of aerosol-related changes in

ACPD
13, 2997–3029, 2013

S.-S. Lee and G. Feingold

precipitation and WP. Since radiative processes have a much longer timescale than the convective time scale, the two-day period is likely not long enough to discern radiative impacts on precipitation and WP. A better understanding of the effect of radiative processes merits further studies with longer-period simulations that are matched to the typical durations of aerosol perturbations.

This study shows that average raindrop terminal velocity increases with increasing aerosol, and is accompanied by decreasing cloud size, increasing updraft strength and the occurrence of heavier precipitation. These changes are consistent with Parodi et al. (2011) and Parodi and Emanuel (2009) who concluded that the raindrop terminal velocity is a physical parameter that, to a large degree, accounts for the cloud system characteristics

In conclusion, the response of a meteorologically constrained cloud system to an aerosol perturbation is an internal readjustment of precipitation pathways to achieve approximately the same amount of integrated precipitation. A by-product of this readjustment is a significant change in updrafts, condensation, and the spatiotemporal evolution of WP and precipitation frequency.

Acknowledgements. The authors thank NOAA's Climate Goal Program for supporting this work and the HPCC for computing support.

References

Albrecht, B. A.: Aerosols, cloud microphysics, and fractional cloudiness, Science, 245, 1227–1230, 1989.

Barker, H. W.: A parameterization for computing grid averaged solar fluxes for inhomogeneous marine boundary layer clouds. Part I: Methodology and homogeneous biases, J. Atmos. Sci., 53, 2289–2303, 1996.

Batterbury, S. and Warren, A.: The African Sahel 25 years after the great drought: assessing progress and moving towards new agendas and approaches, Glob. Environ. Change, 11, 1–8, 2001.

ACPD

13, 2997–3029, 2013

Donner, L. J., Seman, C. J., and Hemler, R. S.: Three-dimensional cloud-system modeling of GATE convection, J. Atmos. Sci., 56, 1885–1912, 1999.
Fan, J., Ruby, L., Li, Z., Hugh Morrison, H., Chen, H., Zhou, Y., Qian, Y., and Wang, Y.: Aerosol impacts on clouds and precipitation in eastern China: results from bin and bulk microphysics, J. Geophys. Res., 117, D00K36, doi:10.1029/2011JD016537, 2012.
Feingold, G. and Kreidenweis, S. M.: Cloud processing of aerosol as modeled by a large eddy simulation with coupled microphysics and aqueous chemistry, J. Geophys. Res., 107, 4687, doi:10.1029/2002JD002054, 2002.
Flossmann, A. I.: The scavenging of two different types of marine aerosol particles using a two-dimensional detailed cloud model, Tellus B, 43, 301–321, doi:10.1034/j.1600-0889.1991.t01-2-00004.x, 1991.
Fridlind, A., Ackerman, A., Petch, J., Field, P., Hill, A., McFarquhar, G., Xie, S., and Zhang, M.: ARM/GCSS/SPARC TWP-ICE intercomparison study, available at: http://science.arm.gov/wg/cpm/scm/scmic6/index.html, last access: 25 October 2009.
Houze, R. A.: Cloud Dynamics, Academic Press, London, England, 573 pp., 1993.
Kim, M.-K., Lau, W. K. M., Chin, M., Kim, K.-M, Sud, Y. C., and Walker, G. K.: Atmospheric teleconnection over Eurasia induced by aerosol radiative forcing during boreal spring, J. Climate, 19, 4700–4718, 2006.
Koren, I., Altaratz, O., Remer, L. A., Feingold, G., Martins, J. V., and Heiblum, R. H.: Aerosol-induced intensification of rain from the tropics to the mid-latitude, Nat. Geosci., 5, 118–122, 2012.
Lee, S. S.: Aerosols, clouds and climate, Nat. Geosci., 4, 826–827, 2011.
Lee, S. S. and Feingold, G.: Precipitating cloud-system response to aerosol perturbations, Geophys. Res. Lett., 37, L23806, doi:10.1029/2010GL045596, 2010.
Lee, S. S., Donner, L. J., Phillips, V. T. J., and Ming, Y: Examination of aerosol effects on precipitation in deep convective clouds during the 1997 ARM summer experiment, Q. J. Roy. Meteorol. Soc., 134, 1201–1220, doi:10.1002/qj.287, 2008a.
Lee, S. S., Donner, L. J., Phillips, V. T. J., and Ming, Y.: The dependence of aerosol effects on clouds and precipitation on cloud-system organization, shear and stability, J. Geophys. Res., 113, D16202, doi:10.1029/2007JD009224, 2008b.
Lee, S. S., Donner, L. J., and Phillips, V. T. J.: Sensitivity of aerosol and cloud effects on radiation to cloud types: comparison between deep convective clouds and warm stratiform clouds over one-day period, Atmos. Chem. Phys., 9, 2555–2575, doi:10.5194/acp-9-2555-2009, 2009.

ACPD
13, 2997–3029, 2013

S.-S. Lee and G. Feingold

Lee, S. S., Feingold, G., and Chuang, P. Y.: Effect of aerosol on cloud-environment interactions in trade cumulus, J. Atmos. Sci., 69, 3607–3632, 2012.

Li, Z., Niu, F., Fan, J., Liu, Y., Rosenfeld, D., and Ding, Y.: Long-term impacts of aerosols on the vertical development of clouds and precipitation, Nat. Geosci., 4, 888–894, 2011.

Orville, R. E., Huffines, G. R., Nielsen-Gammon, J., Zhang, R., Ely, B., Steiger, S., Phillips, S., Allen, S., and Read, W.: Enhancement of cloud-to-ground lightning activity over Houston, Texas, Geophys. Res. Lett., 28, 2597–2600, 2001.

Parodi, A. and Emanuel, K.: A theory for buoyancy and velocity scales in deep moist convection, J. Atmos. Sci., 66, 3449–3463, 2009.

Parodi, A., Foufoula-Georgiou, E., and Emanuel, K.: Signature of microphysics on spatial rainfall statistics, J. Geophy. Res., 116, D14119, doi:10.1029/2010JD015124, 2011.

May, P. T., Mather, J. H., Vaughan, G., and Jakob, C.: Characterizing oceanic convective cloud systems – the Tropical Warm Pool International Cloud Experiment, B. Am. Meteorol. Soc., 154, 153–155, doi:10.1175/BAMS-89-2-153, 2008.

Meehl, G. A., Arblaster, J. M., and Collins, W. D.: Effects of black carbon aerosols on the Indian monsoon, J. Climate, 21, 2869–2882, doi:10.1175/2007JCLI1777.1, 2008.

Morrison, H. and Grabowski, W. W.: Cloud-system resolving model simulations of aerosol indirect effects on tropical deep convection and its thermodynamic environment, Atmos. Chem. Phys., 11, 10503–10523, doi:10.5194/acp-11-10503-2011, 2011.

Morrison, H., Boer, G., Feingold, G., Harrington, J., Shupe, M. D., and Sulia, K.: Resilience of persistent Arctic mixed-phase clouds, Nat. Geosci., 5, 11–17, doi:10.1038/NGEO1332, 2012.

Respondek, P. S., Flossmann, A. I., Alheit, R. R., and Pruppacher, H. R.: A theoretical study of the wet removal of atmospheric pollutants. Part V: The uptake, redistribution and deposition of $(NH_4)_2SO_4$ by a convective cloud containing ice using a two-dimensional cloud dynamics model with detailed microphysics, J. Atmos. Sci., 52, 2121–2132, doi:10.1175/1520-0469(1995)052<2121:ATSOTW>2.0.CO;2, 1995.

Saleeby, S. M. and Cotton, W. R.: A large-droplet mode and prognostic number concentration of cloud droplets in the Colorado state university regional atmospheric modeling system (RAMS). Part I: Module description and supercell test simulations, J. Appl. Meteor., 43, 182–195, 2004.

Solomon, S., Qin, D., Manning, M., Chen, Z., Marquis, M., Averyt, K. B., Tignor, B. M., and Miller, H. L.: Technical Summary, in: Climate Change 2007: The Physical Science Basis, Contribution of Working Group I to the Fourth Assessment Report of the Intergovernmental Panel on Climate Change, edited by: Solomon, S., Qin, D., Manning, M., Chen, Z., Marquis, M., Averyt, K. B., Tignor, B. M., and Miller, H. L., Cambridge University Press, Cambridge, UK and New York, NY, USA, 14.1–996, 2007.

Stevens, B. and Feingold, G.: Untangling aerosol effects on clouds and precipitation in a buffered system, Nature, 461, 607–613, doi:10.1038/nature08281, 2009.

Tao, W.-K., Chen, J.-P., Li, Z., Wang, C., and Zhang, C.: Impact of aerosols on convective clouds and precipitation, Rev. Geophys., 50, RG2001, doi:10.1029/2011RG000369, 2012.

Tompkins, A. M. and Craig, G. C.: Radiative-convective equilibrium in a three-dimensional cloud ensemble model, Q. J. Roy. Meteorol. Soc., 124, 2073–2098, 1998.

van den Heever, S. C., Stephens, G. L., and Wood, N. B.: Aerosol indirect effects on tropical convection characteristics under conditions of radiative-convective equilibrium, J. Atmos. Sci., 68, 699–718, 2011.

Vaughan, G., Schiller, C., Mackenzie, A. R., Bower, K., Peter, T., Schlager, H., Harris, N. R. P, and May, P. T.: SCOUT-O3/ACTIVE High-altitude Aircraft Measurements around Deep Tropical Convection, B. Am. Meteorol. Soc., 88, 647–662, 2008.

Wang, Y., Wan, Q., Meng, W., Liao, F., Tan, H., and Zhang, R.: Long-term impacts of aerosols on precipitation and lightning over the Pearl river delta megacity area in China, 11, 12421–12436, 2011.

Weisman, M. L. and Klemp, J. B.: The dependence of numerically simulated convective storms on vertical wind shear and buoyancy, Mon. Weather Rev., 110, 504–520, 1982.

Xu, K.-M., Cederwall, R. T., Donner, L. J., Grabowski, W., Guichard, F., Johnson, D. E., Khairoutdinov, M., Krueger, S. K., Petch, J. C., and Randall, D. A.: An intercomparison of cloud-resolving models with the atmospheric radiation measurement summer 1997 intensive observation period data, Q. J. Roy. Meteorol. Soc., 128, 593–624, 2002.

Zeng, X., Tao, W.-K., Zhang, M., Peters-Lidard, C., Lang, S., Simpson, J., Kumar, S., Xie, S., Eastman, J. L., Shie, C.-L., and Geiger, J. V.: Evaluating clouds in long-term cloud-resolving model simulations with observational data, J. Atmos. Sci., 64, 4153–4177, 2007.

ACPD
13, 2997–3029, 2013

Aerosol effects on tropical convective cloud properties

S.-S. Lee and G. Feingold

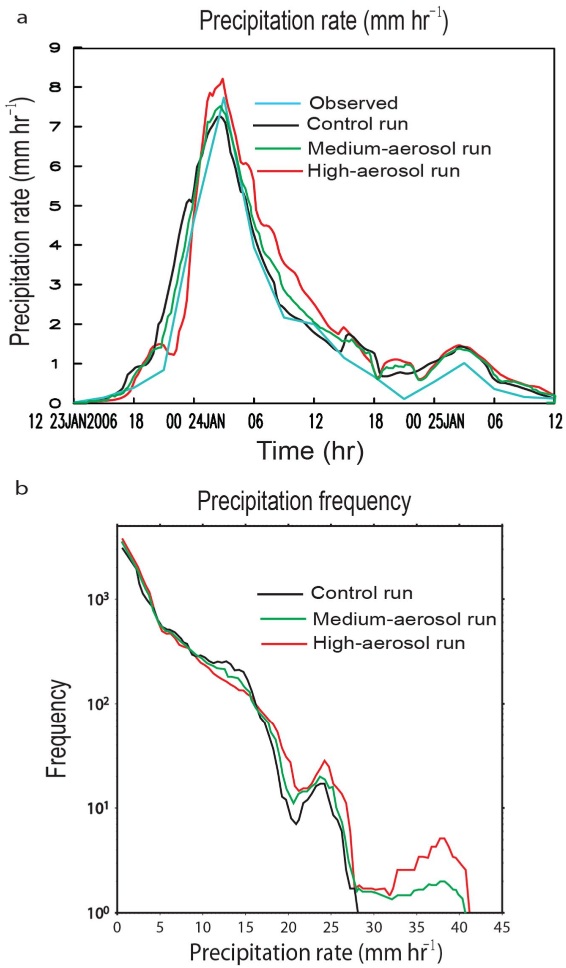

Fig. 1. (a) Time series of precipitation rate (P) and **(b)** frequency distribution of P.

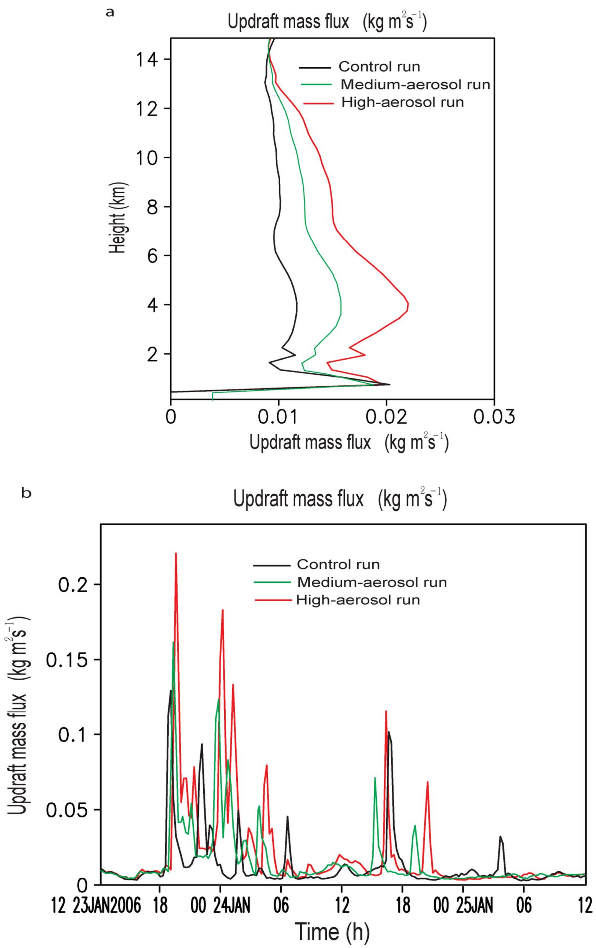

Fig. 2. (a) Vertical distribution of updraft mass fluxes and **(b)** time series of updraft mass fluxes, averaged over grid-cells with positive vertical velocities.

ACPD
13, 2997–3029, 2013

Aerosol effects on tropical convective cloud properties

S.-S. Lee and G. Feingold

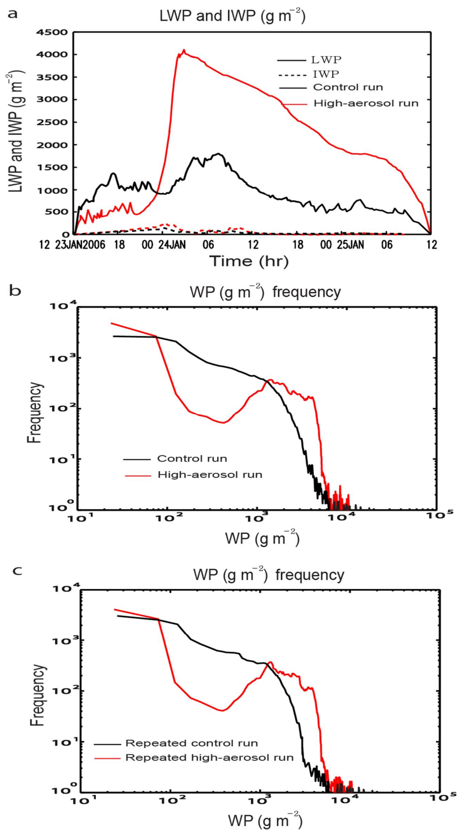

Fig. 3. (a) Time series of liquid-water path (LWP) and ice-water path (IWP) and **(b)** frequency distribution of water-path (WP = LWP + IWP) for the entire simulation period for the control and high-aerosol runs. **(c)** As in **(b)** but for the repeated control and high-aerosol runs with explicit radiation calculations turned off and with the average heating rate from the high-aerosol run (shown in Fig. 11a) imposed on all of grid points in both of the repeated runs.

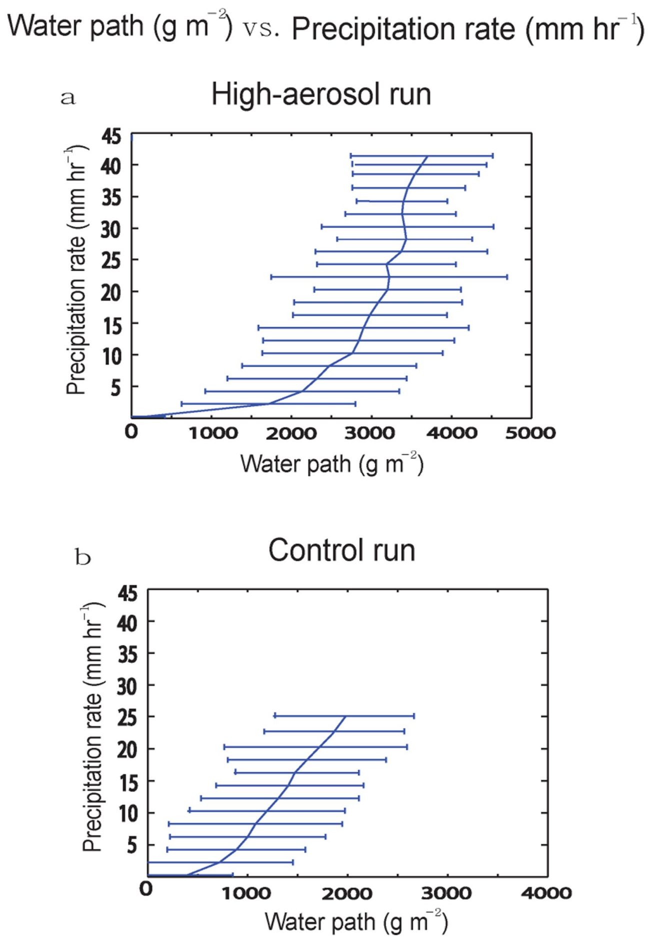

Fig. 4. Averaged WP for **(a)** the high-aerosol run and **(b)** the control run. Vertical bars represent ± one standard deviation.

ACPD
13, 2997–3029, 2013

Aerosol effects on tropical convective cloud properties

S.-S. Lee and G. Feingold

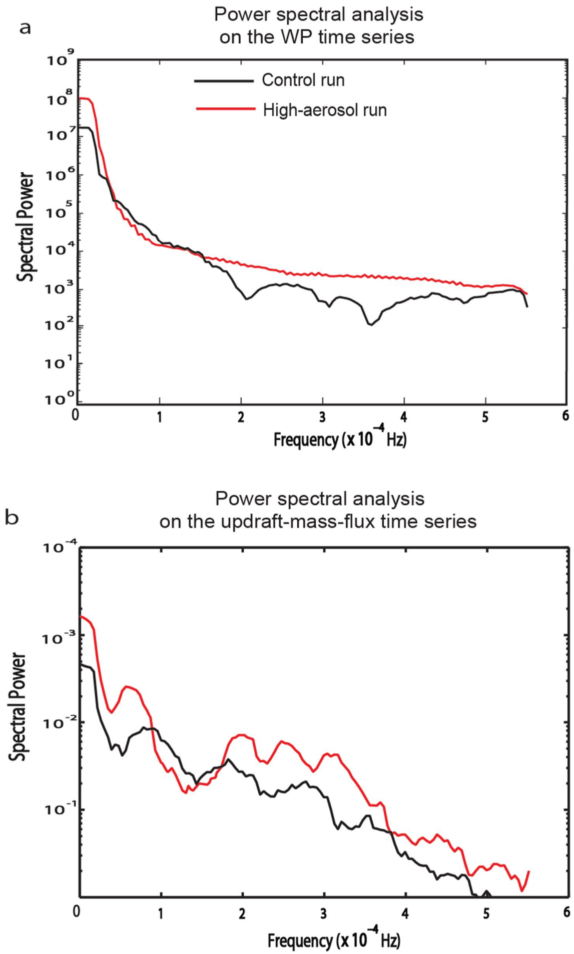

Fig. 5. Power spectral analyses of **(a)** the WP time series and **(b)** the updraft-mass-flux time series.

ACPD
13, 2997–3029, 2013

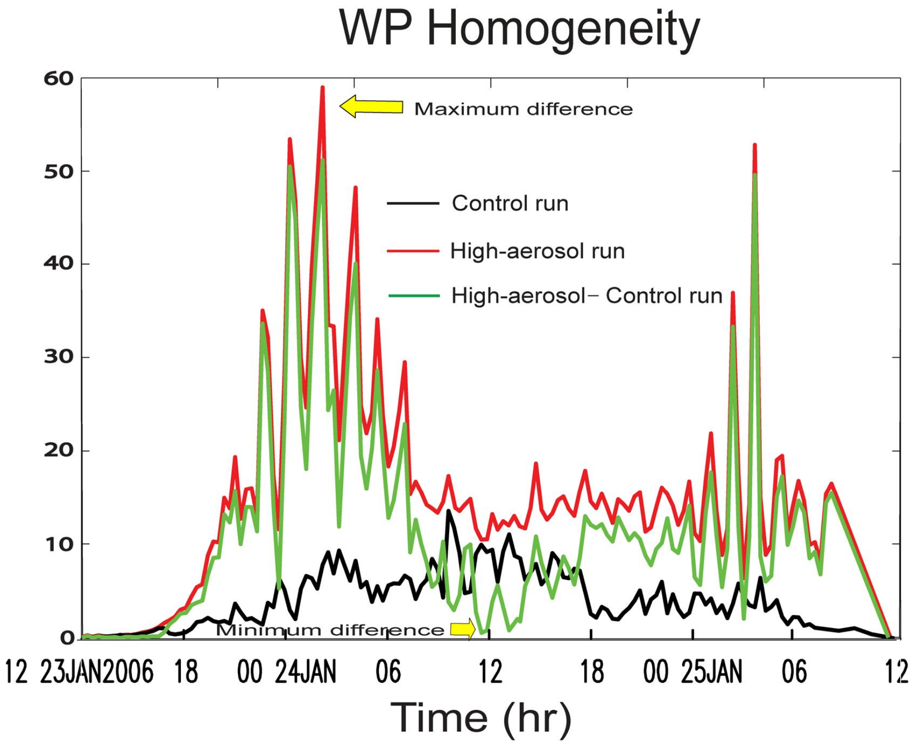

Fig. 6. Time series of the WP homogeneity.

ACPD
13, 2997–3029, 2013

Aerosol effects on tropical convective cloud properties

S.-S. Lee and G. Feingold

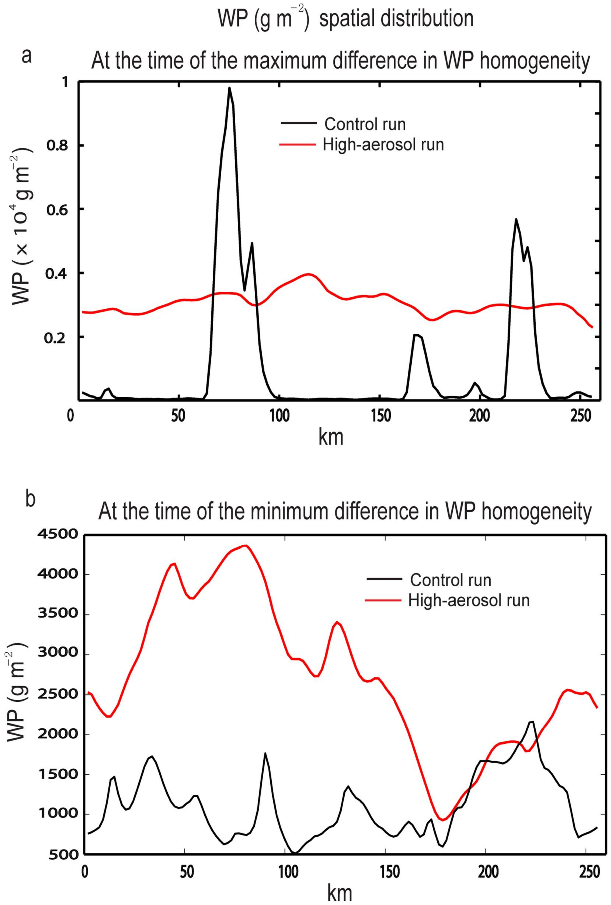

Fig. 7. Spatial distribution of WP over the horizontal domain **(a)** at the time of maximum difference around 03:00 LST on 24 January in the WP homogeneity and **(b)** at the time of minimum difference in the WP homogeneity around 12:00 LST on 24 January.

ACPD
13, 2997–3029, 2013

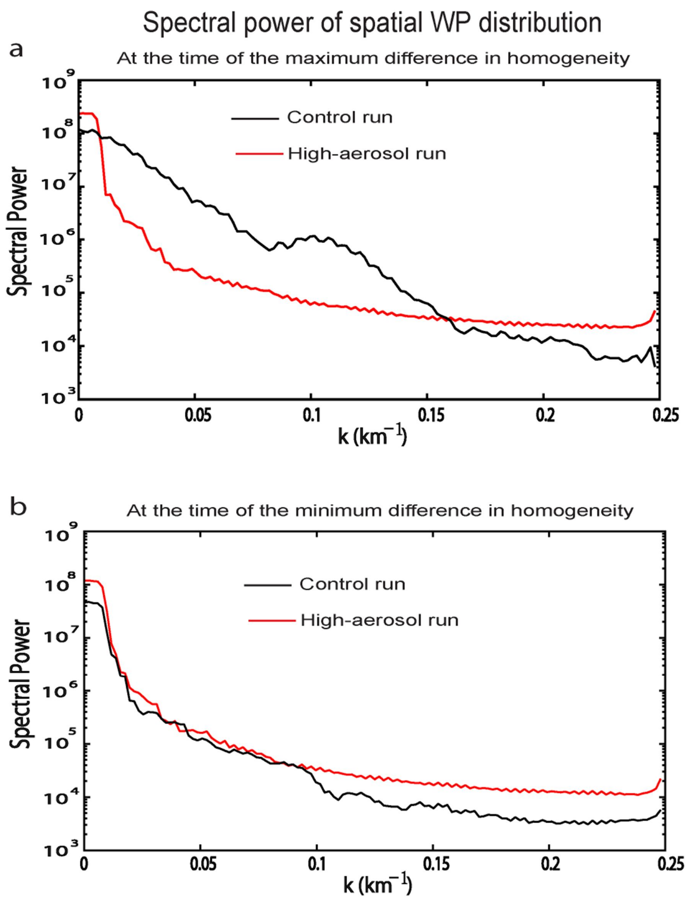

Fig. 8. Spectral power of spatial WP distribution **(a)** at the time of the maximum difference around 03:00 LST on 24 January in the WP homogeneity and **(b)** at the time of the minimum difference around 12:00 LST on 24 January in the WP homogeneity.

ACPD
13, 2997–3029, 2013

Aerosol effects on tropical convective cloud properties

S.-S. Lee and G. Feingold

Title Page
Abstract | Introduction
Conclusions | References
Tables | Figures
◀| |▶
◀ ▶
Back | Close
Full Screen / Esc
Printer-friendly Version
Interactive Discussion

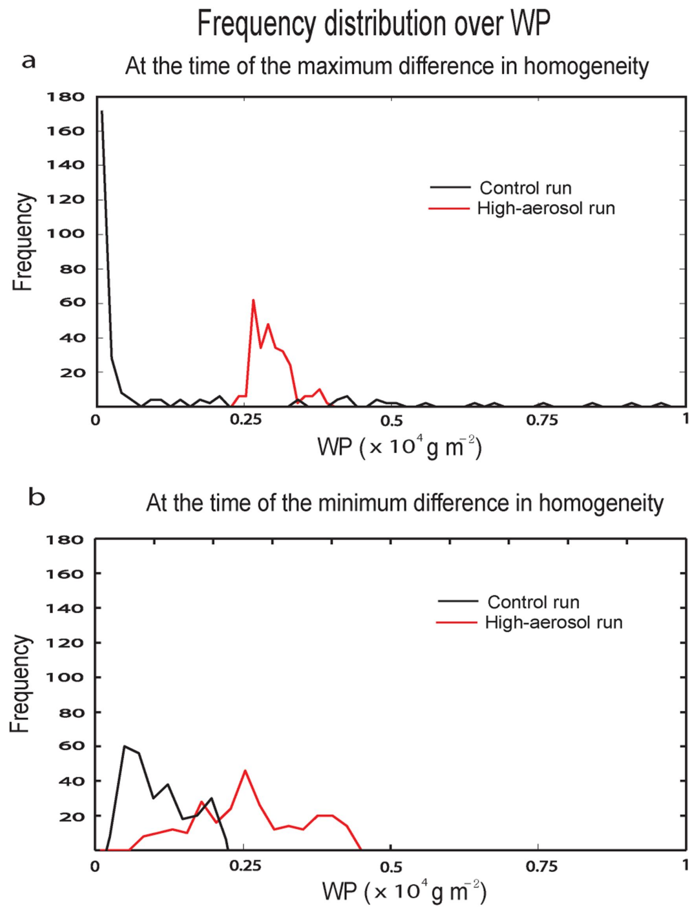

Fig. 9. Frequency distribution of WP **(a)** at the time of maximum difference in homogeneity around 03:00 LST on 24 January and **(b)** at the time of minimum difference in homogeneity around 12:00 LST on 24 January.

ACPD
13, 2997–3029, 2013

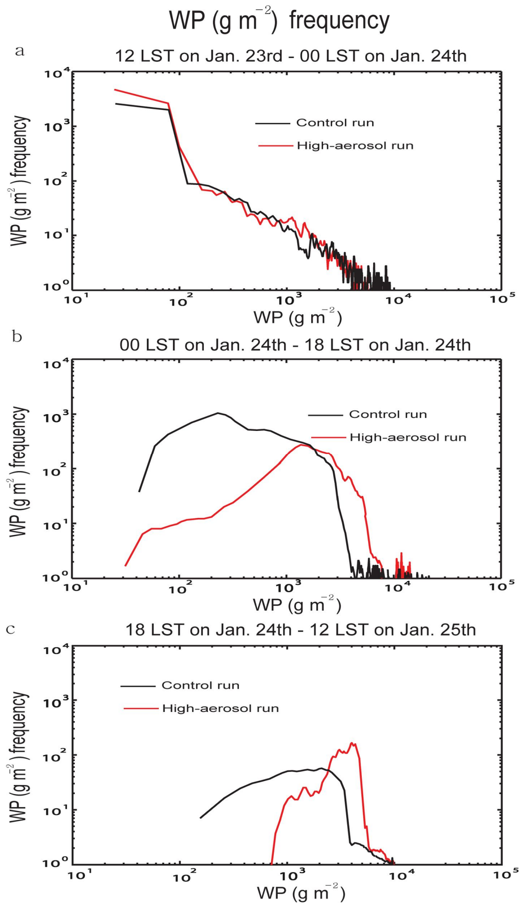

Fig. 10. Frequency distribution of WP over a period **(a)** between 12:00 LST on 23 January and 00:00 LST on 24 January, **(b)** between 00:00 LST on 24 January and 18:00 LST on 24 January, **(c)** between 18:00 LST on 24 January and 12 LST on 25 January.

ACPD
13, 2997–3029, 2013

Aerosol effects on tropical convective cloud properties

S.-S. Lee and G. Feingold

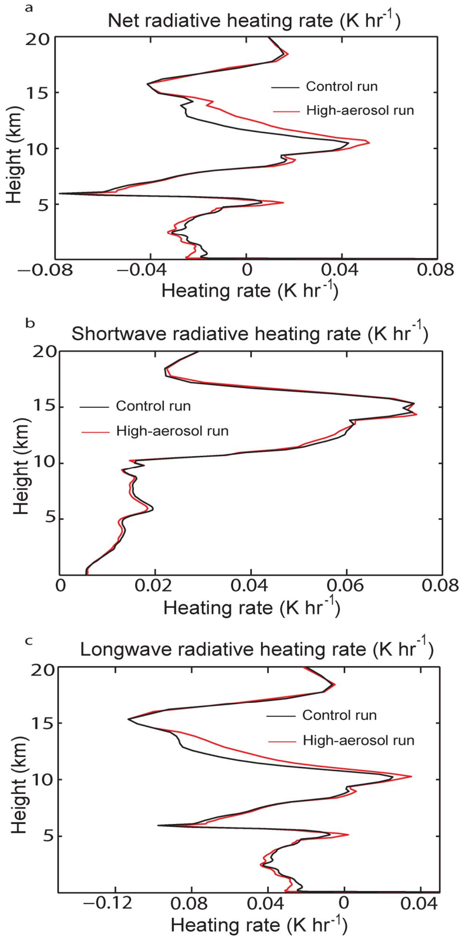

Fig. 11. Vertical distributions of the time- and domain-averaged **(a)** net radiative, **(b)** shortwave radiative and **(c)** longwave radiative heating rates.

ACPD
13, 2997–3029, 2013

Aerosol effects on tropical convective cloud properties

S.-S. Lee and G. Feingold

Title Page
Abstract Introduction
Conclusions References
Tables Figures
◀I ▶I
◀ ▶
Back Close
Full Screen / Esc
Printer-friendly Version
Interactive Discussion

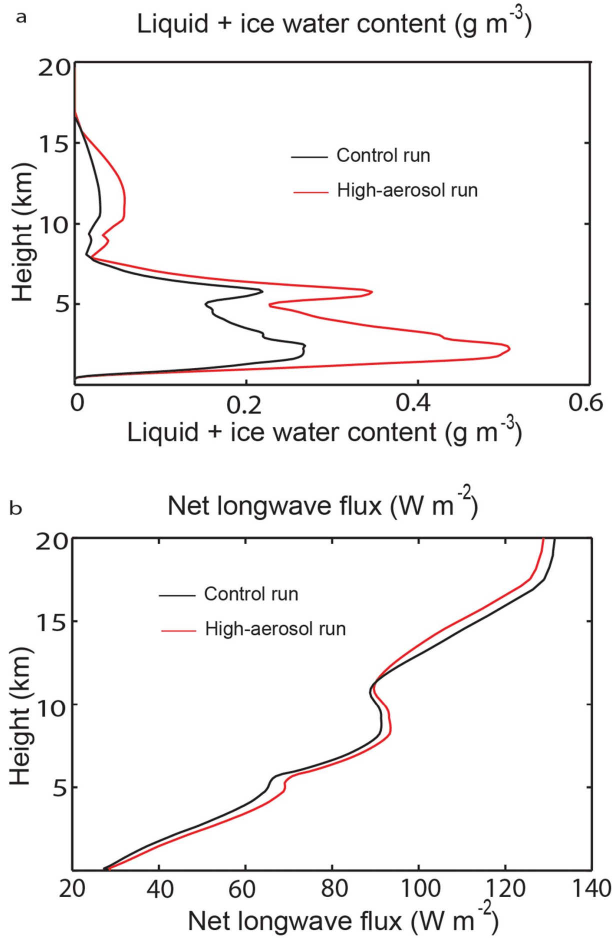

Fig. 12. Vertical distributions of the time- and domain-averaged **(a)** sum of liquid- and ice-water content and **(b)** net longwave flux.

ACPD
13, 2997–3029, 2013

Aerosol effects on tropical convective cloud properties

S.-S. Lee and G. Feingold